metals

MDPI

Article

Study of Adaptation Processes in Tribofilms during Friction of Antifriction Aluminum Alloys for Journal Bearings

Pavel Podrabinnik [1,2,*], Iosif Gershman [3], Alexander Mironov [4], Ekaterina Kuznetsova [4], Anna A. Okunkova [2] and Sergey N. Grigoriev [2]

[1] Laboratory of Innovative Additive Technologies, Moscow State University of Technology "STANKIN", Vadkovsky per. 1, 127055 Moscow, Russia
[2] Department of High-Efficiency Processing Technologies, Moscow State University of Technology "STANKIN", Vadkovsky per. 1, 127055 Moscow, Russia
[3] Department of Scientific Research Programs, Grants and Projects, Railway Research Institute JSC "VNIIZHT", 3rd Mytischinskaya St. 10, 107996 Moscow, Russia
[4] Laboratory of Electric Current Assisted Sintering Technologies, Moscow State University of Technology "STANKIN", Vadkovsky per. 1, 127055 Moscow, Russia
* Correspondence: p.podrabinnik@stankin.ru

Abstract: This paper provides results on the tribological behavior of experimental Al–Sn–Pb–Si–Cu–Mg–Zn aluminum alloys and describes the adaptation phenomena that reduce wear intensity during friction with steel. The main focus is on tribofilm formation, which plays an important role in friction energy dissipation. The alloys were tested in a rig imitating a journal-bearing shaft couple, and the friction surfaces were studied by the scanning electron microscopy, energy-dispersive analysis and X-ray photoelectron spectroscopytechniques. Based on the analysis, a conclusion on processes and tribochemical reactions was made. Compared to the initial state, eight new compounds were found on the friction surface. In the most wear-resistant alloy, magnesium precipitated from a solid solution with the subsequent oxidation. The same process was detected for zinc in the least wear-resistant alloy due to its low magnesium content. Furthermore, $CuSn_3$ and PbS compounds, which require >600 °C temperature to compose, were found in tribofilms, indicating that the rubbing body lost thermodynamic equilibrium during friction. The revealed processes are non-spontaneous and decrease the wear intensity of the alloys, as they are accompanied by negative entropy production and dissipation of friction energy. Stepwise depth XPS analysis also showed the functional levels of the tribofilms.

Keywords: aluminum alloys; journal bearings; friction; tribology; friction surface; tribofilms; adaptation; self-organization; tribochemical reactions

Citation: Podrabinnik, P.; Gershman, I.; Mironov, A.; Kuznetsova, E.; Okunkova, A.A.; Grigoriev, S.N. Study of Adaptation Processes in Tribofilms during Friction of Antifriction Aluminum Alloys for Journal Bearings. *Metals* **2023**, *13*, 1936. https://doi.org/10.3390/met13121936

Academic Editor: Miguel Cervera

Received: 26 October 2023
Revised: 24 November 2023
Accepted: 25 November 2023
Published: 26 November 2023

1. Introduction

Significant costs for overcoming friction forces make the problem of finding more perfect friction pairs constantly relevant [1]. For plain and journal bearings, this task involves the improvement of lubricants [2], bearing design enhancement [3], and the development of new antifriction materials [4]. Along with antifriction behavior, such materials must have sufficient bearing capacity to withstand the load of the counterbody. At the same time, it becomes a barrier to the higher tribological properties all manufacturers strive for.

Mechanical properties are often taken as a criterion for high tribological properties [5]. One major drawback of this approach is ignoring the counterbody while increasing bearing hardness straightforwardly to reduce wear. The addition of hard inclusions such as carbides and oxides may increase the life cycle of a bearing, intensifying the wear rate of shafts as well, which are much more expensive and difficult to replace and repair [6,7]. On the other hand, soft (white) metals, such as tin and lead, significantly increase the tribological

properties but reduce the mechanical ones. Therefore, the use of these metals in bearings tends to be limited. Obviously, the existing requirements for journal-bearing materials are a compromise between tribological and mechanical properties. Replacement bronzes with aluminum alloys are one of the perspectives for journal-bearing improvement. Aluminum is 3.5 times cheaper than copper and ~3 times lighter. Partially, these problems can be solved by using bimetallic and trimetallic journal bearings, where each layer and base perform their function of providing antifriction properties and bearing capacity. However, these bearings are more complicated in production and maintenance.

There are two main antifriction aluminum alloy systems: Al–Sn and Al–Cu [8]. Al–Sn alloys are known for their excellent wear resistance and low friction due to the self-lubricating properties of tin. These alloys are widely used in journal bearings, bushings, and other sliding or rotating components where reducing friction and wear is critical. Usually, these alloys contain 7–20% tin [9,10]. Meanwhile, Al–Cu alloys have increased strength, wear resistance, and load-bearing capacity compared to pure aluminum [11]. Such materials work according to the Charpy principle, in which an oil-retaining layer is created on the surface due to a large number of small hard inclusions in a soft aluminum matrix. New antifriction materials are actively being developed based on these two systems and their additional alloying [12–15].

Traditional ways have almost exhausted the possibilities for a significant improvement in the quality of friction pairs, and, therefore, many studies have begun to focus on the study of surface tribofilms [16–18]. At the same time, it has been written in articles on friction for more than half a century that tribological characteristics are determined by the processes occurring on rubbing surfaces [19]. However, only a few studies have used these findings to develop new tribological materials. Bershadsky et al. [20] showed that non-spontaneous processes with negative entropy production decrease the wear rate. This principle was used for developing wear-resistant materials for sliding electrical contacts [21], journal bearings [22], and coatings for cutting tools [23]. Thermodynamic self-organization was also described for metals during fatigue [24].

Following this principle, the running-in stage becomes the final operation in the bearing production chain that ensures optimal tribological properties [16]. The formed tribofilms determine the tribological behavior of the material. The tribofilms are the result of different processes that take place during friction, which are not fully studied. Starting in the middle of the 20th century, the number of studies on tribofilms has steadily increased, describing the influence of tribochemical and tribophysical phenomena on friction. Nakayama et al. described the processes of triboemission of elementary particles, the formation of tribomicroplasma, surface charge, and other tribochemical reactions [25]. It is reported that the phenomenon occurs not only in the place of direct contact between two bodies but also in the areas around it. Nonetheless, tribochemical processes are expected to have a greater impact on friction and attract more attention. Those processes include common phenomena such as oxidation [26], the Rehbinder effect [27], or tribocatalysis. Kubo et al. noted the possibility of the formation of tribofilms on the surface of silicon oxide SiO_2, which contribute to the superfluidity of a liquid due to the formation of layers of colloidal silicon oxide and hydrophilic hydrates [28]. Kuzharov et al. showed that tribochemical reactions play a decisive role in [29]. The authors noted that during friction, a tribofilm (a "servovite" film) is formed, which provides wear-free mode and super-friction. The possibility of forming tribofilms that improve tribological properties due to tribochemical reactions formed the basis for various additives that reduce wear and friction coefficients [30–32]. One of the most common additives is zinc dialkyl dithiophosphate (ZDDP), which is characterized by stable tribofilm formation and significantly improves the tribological behavior of the friction pair [33]. During friction, tribochemical reactions occur with the formation of zinc polyphosphates and sulfides, which have high tribological properties. Phosphorus and sulfur for such compounds are taken from the lubricant, which means that all objects of the tribosystem are involved in the formation of tribofilms.

ZDDP and other additives, such as molybdenum disulfide (MoS_2), contribute to wear reduction due to the physical properties of the material or the compounds formed on the surface as a result of reactions. On the other hand, a decrease in wear intensity can be achieved by redistributing the friction energy. Such processes are the basis of tribofilms formed during self-organization during friction [22].

Thermodynamically, the decrease in wear rate can be achieved by reducing the production of entropy during friction through tribofilm formation [34]. Following this approach, a tribosystem is considered from the standpoint of non-equilibrium thermodynamics and the theory of self-organization [22]. The main idea is to reduce the wear rate with a decrease in entropy production. A noticeable decrease in entropy production can occur during self-organization and the formation of tribofilms. After self-organization, non-spontaneous processes can occur stably, i.e., physical and chemical processes accompanied by an increase in free energy and a negative production of entropy. Once the equilibrium of two bodies that were initially in different states is reached, the thermodynamic forces are equalized, and flows of energy and substances disappear (Figure 1a). If tribofilms are not formed during friction, then the energy and potentials will be distributed over the body by a monotonically decreasing function of the distance from the friction surface (Figure 1b). During friction, the amount of energy may be too large to dissipate in regular ways, such as through thermal and electroconductivity or diffusion. It might result in catastrophic wear and scoring or the formation of new structures on friction surfaces [35]. In the latter case, a zone of predominant energy dissipation appears, i.e., friction energy is redistributed in the rubbing body with the formation of tribofilms (Figure 1c).

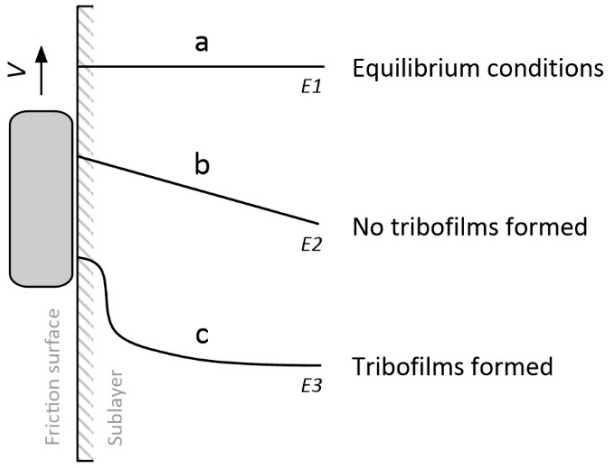

Figure 1. Energy dissipation during friction: (**a**) at equilibrium conditions; (**b**) without tribofilms; (**c**) with tribofilms formed [34].

Before self-organization, such processes existed only as unstable fluctuations. After self-organization, the production of entropy is less than under the same conditions but without self-organization [36]. In [22], it is reported that a decrease in wear is possible when non-spontaneous tribochemical reactions occur, which are accompanied by negative entropy production, leading to a decrease in the total entropy production in the system. This idea is of great interest since, although friction is an artificial process, the reaction to friction is a natural process. However, objective observation of the non-spontaneous processes during friction is impossible. Often, tribofilms are the only evidence of such processes.

This work is part of research aimed at studying tribolayers and their influence on the friction of aluminum alloys with steel.

2. Materials and Methods

2.1. Raw Materials

For the research, eight Al–Sn–Pb–Si–Cu–Zn–Mg aluminum alloys (AA) were used (Table 1). Tin is the main and most expensive component in aluminum-based antifriction alloys for plain bearings (Al20Sn1Cu, Al12Sn4Si1Cu, and Al40Sn1Cu) without an antifriction layer. However, such alloys are used only in bimetallic plain bearings due to their low mechanical properties. To obtain an alloy for monometallic journal bearings in this study, the tin content was varied from 11.0% to 5.4%, while complex alloying was made to increase the material's tendency to self-organize.

Table 1. The composition of the aluminum alloys.

Alloy	Composition, % Mass.								Impurities, % Mass.
	Sn	Pb	Cu	Zn	Mg	Si	Al	Ti	Fe
AA1	11.0	2.6	3.9	2.6	0.0	0.1	bal.	0.04	0.2
AA2	9.8	2.5	4.5	2.4	1.2	0.6	bal.	0.03	0.3
AA3	9.6	3.2	4.9	4.4	0.3	0.1	bal.	0.02	0.3
AA4	8.7	3.2	3.4	2.9	0.4	0.5	bal.	0.03	0.1
AA5	7.6	3.3	4.0	0.5	0.07	1.0	bal.	0.05	0.1
AA6	6.4	3.0	4.1	1.9	1.4	0.9	bal.	0.03	0.2
AA7	5.8	2.7	4.1	2.3	1.5	1.5	bal.	0.04	0.1
AA8	5.4	2.6	3.5	2.3	1.7	0.8	bal.	0.04	0.1
Bronze	5.1	18.5	bal.	4.9	-	0.1	0.1	-	<0.4

Lead, due to its limited dissolution, is prone to segregation in aluminum, and the predominant formation of low-melting eutectic with tin was introduced in an amount of 2.5–3.2%. According to the state diagram, lead is capable of forming low-melting eutectics with tin, which promotes sliding when friction conditions become more severe.

An increase in the mechanical properties of the alloys was achieved by alloying with copper at a level of 3.4–4.9%. Part of the copper enters into a solid solution with aluminum (up to 0.6%), and the rest of the copper forms a network of $CuAl_2$ solid inclusions due to non-equilibrium crystallization. Silicon was also introduced to strengthen alloys, improve castability, and reduce the risk of hot cracks. When the solubility limit in aluminum is exceeded (0.05%), silicon is released in the form of brittle crystals, reducing the ductility of the alloy. Therefore, silicon was introduced in the range of 0.1–0.6%.

Zinc is an important alloying element in high-strength aluminum alloys and dissolves in aluminum up to 8%. It was varied from 0.5 to 4.4% to assess the effect on properties.

Magnesium dissolves up to 1.9% in aluminum, increasing its strength and ductility. However, above this value, there is a possibility of the formation of intermetallic compounds such as Mg_3Al_4 and Mg_2Si, among others, characterized by brittleness and hardness. In view of this, to assess the effect on mechanical and tribological properties, magnesium was introduced in the range of 0.0 to 1.7%.

Titanium was introduced into the alloy during casting as a degasifier and modificator for grain refinement.

In addition to the direct effect on the properties, complex alloying of alloys is necessary, among other things, to increase the likelihood of loss of thermodynamic equilibrium of the material during friction, which is a necessary condition for self-organization. Therefore, alloying components with a known effect on properties were selected for the alloy with contents that provide a compromise between mechanical and tribological properties.

The aluminum alloys were obtained by casting in cast iron forms with the following heat treatment, explaining the low iron contents. The ingots were machined to produce "stars" with five friction surfaces with a radius of 20 mm (Figure 2). The friction surface roughness of aluminum and steel samples before tribological tests was Ra = 0.6–0.8 μm and was controlled by a Hommelwerke T8000 profiler (Hommelwerke GmbH, Schwenningen, Germany).

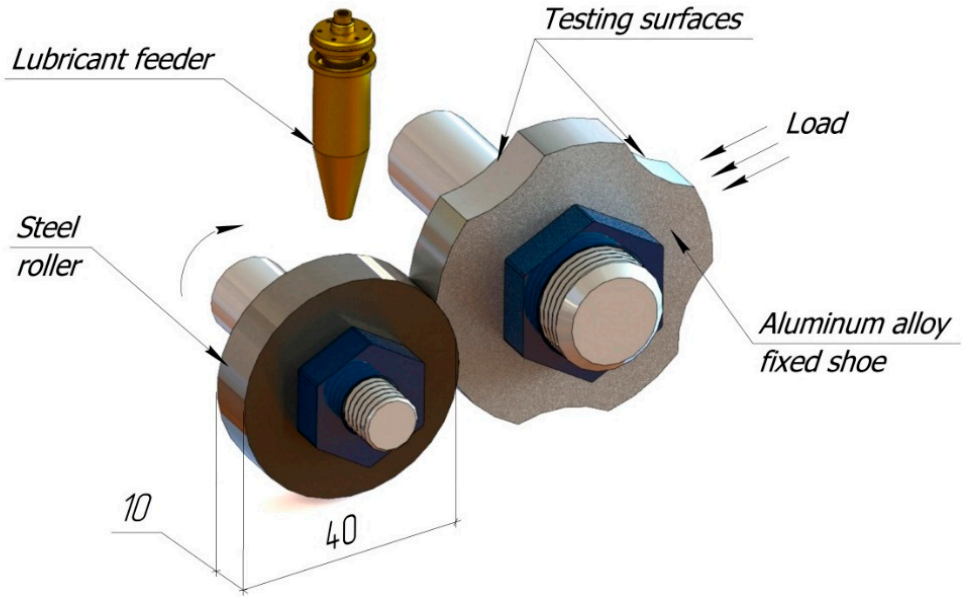

Figure 2. Kinematic configuration of the friction mechanism experiments.

2.2. Tribological Tests

Tribological experiments were performed according to the shaft-block kinematic scheme of the friction machine SMC-2 (Tochmashpribor, Ivanovo, Russia) under mixed lubrication conditions for 40 h at a constant rotation speed of 500 rpm and a load of 617 N (Figure 2). Apart from aluminum samples, 38HN3MA steel was used as a counterbody (Table 2), and M14V2 oil was used as a lubricant (Table 3). For reference, commercially available antifriction bronze Cu–4Sn–4Zn–17Pb (Table 1) was also tested.

Table 2. The composition of the 38HN3MA steel.

	Composition, % Mass.									
38HN3MA Steel	**C**	**Si**	**Mn**	**Ni**	**S**	**P**	**Cr**	**Mo**	**Cu**	**Fe**
	0.36	0.25	0.35	2.90	<0.025	<0.025	1.0	0.3	0.24	bal.

Table 3. The composition of the M14V2 lubricant.

CH_2	**S**	**Ca**	**Al**	**Mg**	**Zn**	**Si**	**P**	**Mo**	**Fe**	**Cl**
98.3%	1.16%	0.23%	910 ppm	648 ppm	590 ppm	514 ppm	499 ppm	126 ppm	65 ppm	50 ppm

After the tests, the specimens were washed in water and carbon tetrachloride to remove all the lubricant residues and wear products. The final cleaning took place in an ultrasonic bath of chemically pure acetone. The aim of this procedure was to expose areas where non-spontaneous or other important char processes could possibly take place, as they may be hidden by polymerized films.

The wear of the samples was assessed by weighing on an electronic laboratory balance GR-300 (A & D, Tokyo, Japan) with a weighing accuracy of up to 0.0001 g. The tests were carried out three times for each alloy.

2.3. Chemical and Microstructural Characterization

The composition of the alloys after casting was measured by the emission spectrometer Spectrolab-S (Spectro Analytical Instruments GmbH, Kleve, Germany).

The microstructure of the alloys and friction surfaces was studied using a scanning electron microscope(SEM), the Tescan Vega 3 (Tescan, Brno, Czech Republic). The ele-

mental analysis was performed using the X-Act energy dispersive analysis (EDX) detector (Oxford Instruments, Abingdon, UK) at an accelerating voltage of 20 kV to induce all the characteristic lines of the main elements.

The friction surfaces of the aluminum alloys were also analyzed using photoelectron spectroscopy (XPS) by Thermo Scientific K-alpha (Thermo Fisher Scientific, East Grinstead, UK) with the Al Kα source to study bonds. All the samples were preliminarily cleaned by 100 nm depth Ar^+ ion etching at 4 keV with a 45° incidence angle. The sputtering rate was estimated by measuring time spent on 1 μm depth erosion. The latter was measured by scanning electron microscopy.

3. Results and Discussion

3.1. Tribological Behavior of the Alloys

The main registered tribological parameters included the coefficient of friction (CoF), linear wear of the AA block, and wear loss of the roller (Table 4). The latter two values were taken as criteria to compare the tribofilms of the best aluminum alloy AA7 and the worst AA4 alloy.

Table 4. The results of the tribological tests.

Alloy	Tribological Parameters		
	Steel Wear, mg	Linear Wear of the Alloy, mm	CoF
AA1	0.6 ± 0.1	0.0025 ± 0.0004	0.020 ± 0.003
AA2	0.7 ± 0.1	0.0015 ± 0.0003	0.015 ± 0.002
AA3	2.1 ± 0.3	0.0042 ± 0.0007	0.019 ± 0.003
AA4	0.8 ± 0.1	0.0051 ± 0.0006	0.022 ± 0.002
AA5	0.8 ± 0.1	0.0011 ± 0.0002	0.026 ± 0.004
AA6	1.0 ± 0.2	0.0019 ± 0.0004	0.014 ± 0.002
AA7	0.6 ± 0.1	0.0008 ± 0.0002	0.018 ± 0.003
AA8	0.7 ± 0.1	0.0011 ± 0.0002	0.017 ± 0.003
Bronze	4.0 ± 0.3	0.0017 ± 0.0003	0.016 ± 0.004

The wear values were correlated with the content of the soft inclusions, indicating the removal of white metals as the main wear mechanism. The more tin in the alloy, the higher the wear (Figure 3a). Hard inclusions contributed to the wear resistance of the alloy (Figure 3b).

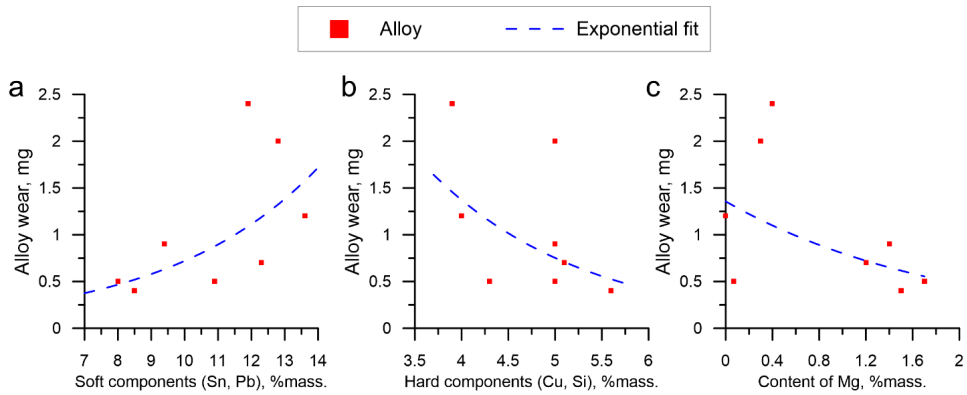

Figure 3. The dependence of alloy wear on the content of (**a**) soft inclusions, (**b**) hard inclusions, and (**c**) magnesium.

3.2. The State of Material before Friction

Self-organization processes and tribofilms are sensitive to testing environments and rigs. Since the formation of tribofilms is a response of the system to certain friction conditions, the running-in stage and experiments should be carried out under conditions closest

to reality. The tribopair must adequately reproduce the operating conditions of the shaft and the journal bearing in terms of load, lubrication, speed, distance, geometry, contact area, and temperature [37]. Therefore, express tests such as scratching are not representative.

To track the tribofilm formation processes, the microstructure of the aluminum alloys before friction was studied. All the alloys shared one microstructure, as presented in Figure 4. The matrix contained solid inclusions based on copper ($CuAl_2$, θ-phase) and silicon. There were also soft inclusions based on tin, lead, and their eutectics.

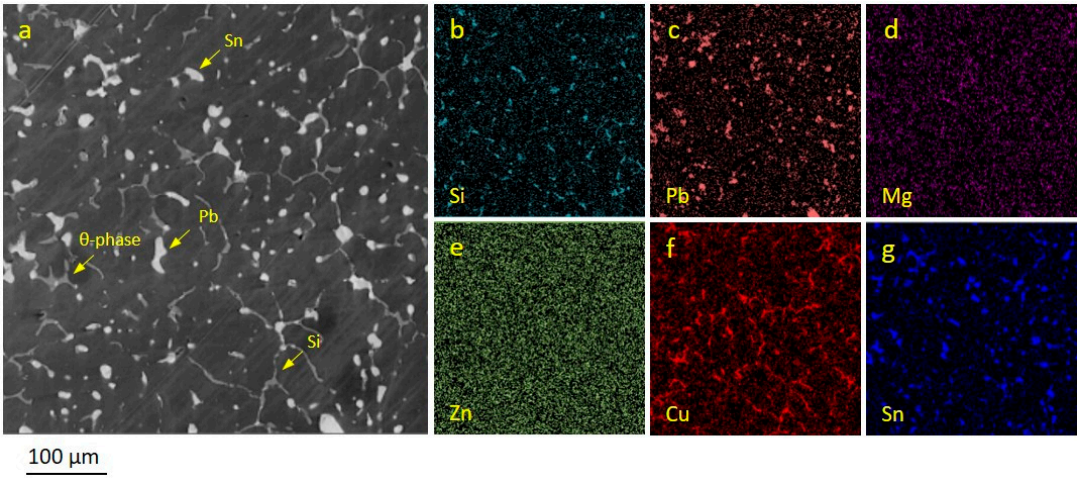

Figure 4. The typical microstructure of aluminum alloys before friction: (**a**) SEM image and the EDX-maps of (**b**) silicon, (**c**) lead, (**d**) magnesium, (**e**) zinc, (**f**) copper, and (**g**) tin.

3.3. SEM Analysis

The friction surface of the AA7 is presented in Figure 5. Tin and lead were spread generously over the surface (Figure 5c,g). The raised content of O and C was also detected by EDX (Figure 5i,j). Apart from air, lubricant is the main source of these elements. By polymerizing on the surface, the lubricant became the basis for the tribofilms. Furthermore, areas with increased concentrations of magnesium up to 13% mass were observed (Figure 5d). Before friction, there was only 0.2–0.4% mass of magnesium uniformly dissolved in the matrix and soft inclusions. Therefore, it could be suggested that magnesium is capable of precipitating from the aluminum matrix. These areas were also enriched with oxygen and carbon. EDX maps of sulfur and lead shared the same pattern, indicating the possibility of creating a new bond after friction. The EDX results for the whole visible area are given in Table 5. Intensive smearing of tin and lead stands behind the increased content of soft metals on the friction surface.

Despite having more soft inclusions, AA4 demonstrated the lowest wear resistance. Soft metals were removed during friction, which resulted in more severe friction. This is evidenced by cavities, the bottoms of which are shaped by aluminum matrix grains. The size of the cavities corresponds to the dimensions of soft inclusions before friction (Figure 6). The extrusion of tin on the surface was caused by temperature and plastic deformation. The temperature could increase and contribute to the plasticity of the metals in the local areas due to a larger number of seizure centers. The exposed surfaces of the alloy were oxidized, as evidenced by the brittle fracture. Thus, the removal of soft metals was the main mechanism of wear loss for the AA4 alloy.

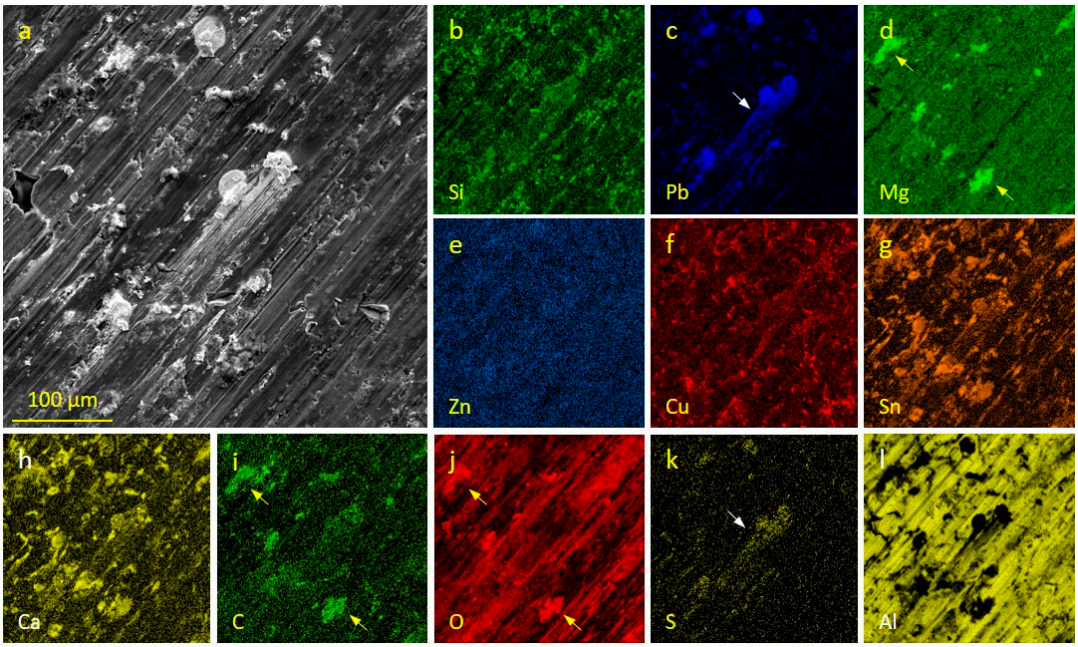

Figure 5. Friction surface of the AA7 alloy: (**a**) SEM image; EDX maps of (**b**) silicon; (**c**) lead; (**d**) magnesium; (**e**) zinc; (**f**) copper; (**g**) tin; (**h**) calcium; (**i**) carbon; (**j**) oxygen; (**k**) sulfur; and (**l**) aluminum.

Table 5. The results of the EDX analysis of the AA7 friction surface.

Object	Elements Composition, % Mass.											
	Al	Sn	Pb	Cu	Si	Zn	Mg	C	O	Fe	S	Ca
Surface before friction	77.7	3.7	2.1	2.9	1.8	2.2	0.3	5.1	3.9	-	-	-
Surface after friction	39.5	3.9	4.7	2.0	0.4	1.5	0.6	31.3	15.5	0.2	0.3	0.1
Change, %	50.8	105.4	223.8	69.0	22.2	68.2	200	611.8	397.4	-	-	-

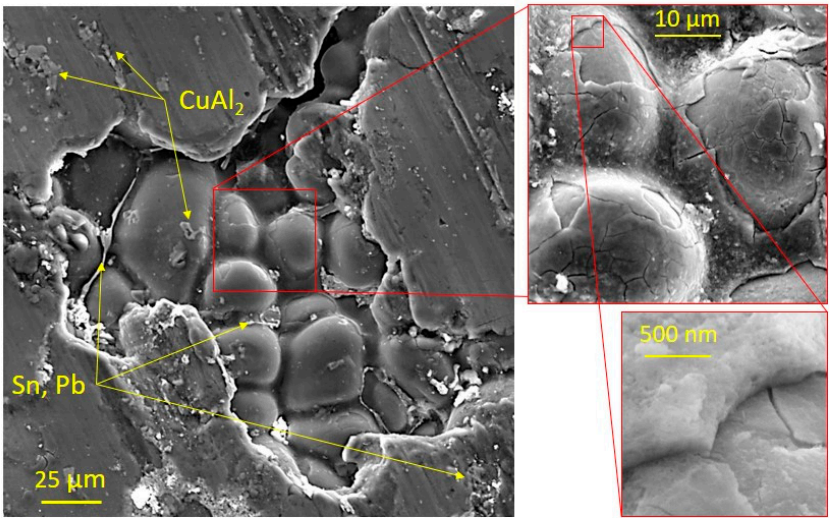

Figure 6. A cavity on the friction surface of the AA4 alloy soft inclusions were removed from.

More severe friction caused the formation of tribofilms that were different from the AA7 alloy. Firstly, there are areas with increased zinc concentrations instead of magnesium (Figure 7). This is attributed to the initial alloying of materials. The AA4 alloy contained 4.5 times less magnesium. In addition, the copper-based array is more pronounced in the

alloy, which takes on the load of the counterbody, increasing wear resistance. It also gives relief to the friction surface and performs the lubricant-retaining function.

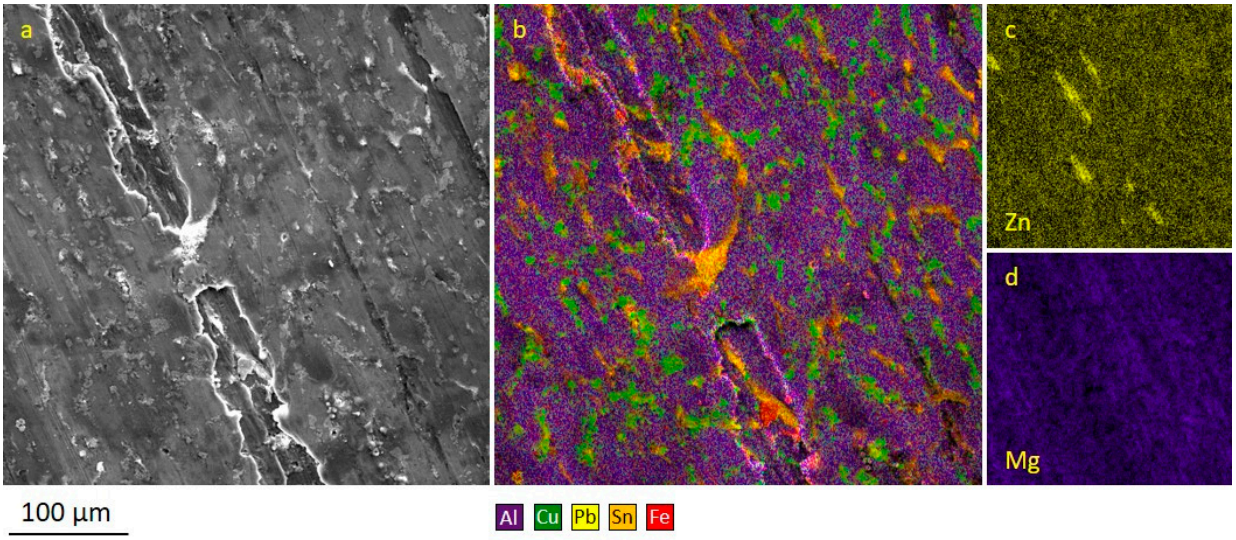

Figure 7. Friction surface of the AA4 alloy: (**a**) SEM image; EDX maps of (**b**) aluminum, copper, tin, lead, and iron; (**c**) zinc; and (**d**) magnesium.

3.4. XPS Analysis

While EDX gives important information on element composition and their local arrangement, XPS extends knowledge on tribochemical processes by providing data on new bonds formed after friction. However, the results can be compared only qualitatively because EDX collects data up to 3 microns deep, while XPS is a surface-sensitive technology that involves only up to 30 atomic layers, depending on the material. This factor is critical for studying tribofilms.

Compared to the initial state, both alloys had significant changes (Figure 8). As expected, the intensity of the oxygen and carbon peaks increased a lot due to interaction with the lubricant and air. In addition, the Fe peak (~707.6 eV) demonstrated intensive mass transfer of steel debris from the counterbody.

A considerable difference is observed in the 1304.3 eV region, which stands for magnesium and its bonds. Before friction, the peak was small. However, a strong peak is already observed on the friction surface of the AA7 alloy, the intensity of which is an order of magnitude higher. The intensity of the magnesium peak in the AA4 is comparable to the state before friction. It confirms the conclusion about magnesium precipitation in AA4 and supports the EDX results.

In contrast, the AA4 alloy demonstrated the highest Zn peak at 1021 eV. In contrast to the AA7 alloy, zinc precipitated from the solid solution, although to a lesser extent than magnesium in AA7.

AA7 had a significant intensity of the tin peak (~485 eV) due to its smearing over the surface. Because of this, the aluminum peak (~75 eV) is less pronounced since a significant area was covered with soft metals. In the AA4, due to more intense friction and active consumption of soft structural components, the tin peak is smaller, and lead (~138 eV) is found on the surface to a greater extent.

For a more detailed study of the tribochemical transformations, high-resolution XPS spectra of the detected elements were obtained. Figure 9a shows the photoelectron spectrum of aluminum Al 2p. In the initial state, upon decomposition of the X-ray spectral contour, four peaks are observed with binding energies of 72.9 eV and 73.3 eV, identified as aluminum, and 75.7 eV and 76.2 eV, corresponding to aluminum oxide Al_2O_3.

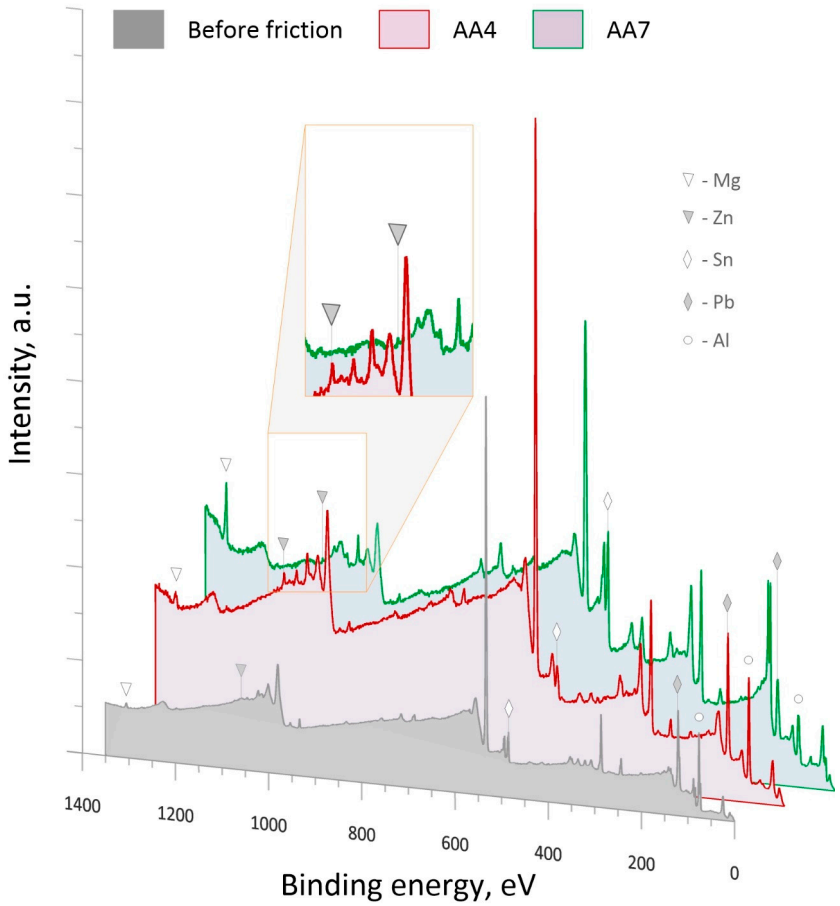

Figure 8. XPS survey spectra of the AA4 alloy, AA7 alloy, and aluminum alloy before friction.

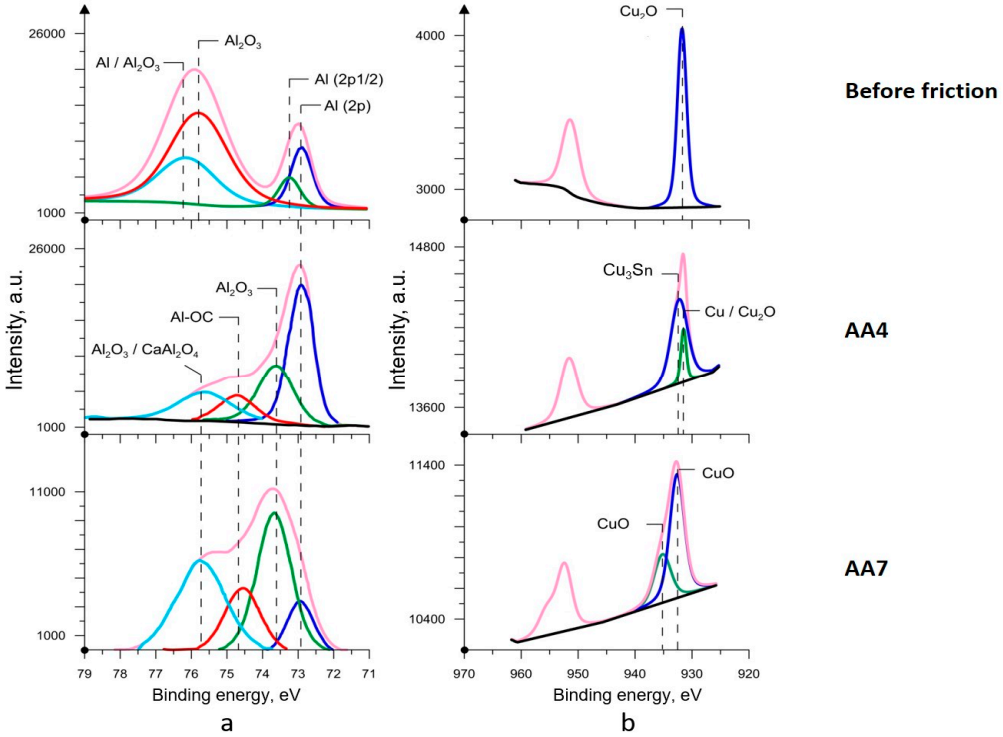

Figure 9. High-definition XPS spectra of (**a**) Al and (**b**) Cu.

After friction, the main aluminum peak was observed at 73.9 eV. The splitting between this and the nearest peak was 0.7 eV, which corresponds to the Al_2O_3 compound for the second peak. However, the Al_2O_3 doublet is no longer observed (75.7 eV and 76.2 eV). In the first case, the aluminum carboxylic compound Al–OC in various stoichiometry is most likely formed [38]. Presumably, this led to a shift towards lower energies of the fourth peak with a binding energy of 75.7 eV, corresponding to aluminum oxide. Also, this peak can be interpreted as a compound of $CaAl_2O_4$ [39].

Changes were also detected for copper (Figure 9b). In the initial state, the dominant compound was $CuAl_2$ coated with an oxide film (CuO, ~932.9 eV). After friction, the 932.6 eV and 933.1 eV peaks were found in the AA4 alloy. The first was identified as copper oxide II, Cu_2O [40]. Peaks at 933.1–933.2 eV can be identified as tricopper stannide Cu_3Sn [41]. Normally, it would also be taken as Cu_2O or Cu^0. However, copper oxide already exists as a 932.6 eV peak, while the appearance of metal copper is hard to suggest after intense friction. The system contains both elements needed to make such a compound. Furthermore, if the thermodynamic equilibrium is lost, such reactions may take place at different conditions compared to the normal state.

In the AA7 alloy, the peaks were shifted towards higher energies. The peak at 933.7 eV was identified as CuO [42]. The peak at 936.1 eV also corresponds to the Cu^{2+} state and was identified as CuO [43]. Copper fluoride, CuF_2, is also reported to have this binding energy [44]. However, there are no sources of fluorine in the tribosystem. Thus, in general, in all alloys, copper and inclusions based on it undergo oxidation. Due to more intense friction in the AA4 alloy, an intermetallic compound, Cu_3Sn, was found, which, according to Franke et al., is formed according to the following Formula (1) [45]:

$$3Cu + Sn \xrightarrow{676\ ^\circ C} Cu_3Sn \quad (1)$$

This reaction may be the result of diffusion in the solid state. With intense friction, elevated temperatures, and large loads, the flow conditions can shift towards more achievable ones, making the reaction possible. The diffusion process includes the mutual diffusion of Cu and Sn atoms on a microscopic scale, which leads to the formation of Cu_3Sn compounds at the interface. This compound is used in the form of solid inclusions in B83 babbitt and has a positive effect on reducing wear intensity as a hard inclusion [46].

The deconvolution of the Sn 3d5 high-resolution spectrum of tin in the initial state revealed the presence of two Gaussians (Figure 10a). The most intense peak had a binding energy of 484.7 eV, which corresponds to metallic tin [47]. Partially, tin is found in the form of SnO_2 (487.1 eV) [48]. The AA7 alloy inherited the same pattern after friction (Figure 10a). Metallic tin remained at 484.7 eV with a higher intensity. The SnO_2 peak shifted to 487.2 eV. Its intensity was raised, and the full width at half maximum (FWHM) parameter was also broadened from 1.8 eV to 2.7 eV, suggesting the presence of tin in bonds different from Sn (IV).

For the AA4, the fitting of the XPS spectra revealed a different pattern (Figure 10a). The binding energy of metallic tin remained at the same level of 484.7 eV but suffered a twofold decrease in intensity and became the lowest. Tin (IV) oxide, with a binding energy of 487.2 eV, prevails on the friction surface. In addition to these two states of tin, a peak with a binding energy of 488.6 eV was also found. It was interpreted as tin dioxide SnO_2 as the most likely compound and closest to the ones described in the literature.

When taking the XPS spectrum of lead in the 4f range, a doublet of Pb ($4f_{7/2}$ and $4f_{5/2}$) is observed (Figure 10b). Before friction, the most intense component, Pb $4f_{7/2}$, of the spectral contour had a 136.6 eV peak, representing metallic lead Pb^0 [49]. The second peak was much less intense and had a binding energy of 137.7 eV. It covered a wide binding energy range, with an FWHM parameter of 2.9 eV. This peak corresponds to lead oxides in different stoichiometry, but it is hard to distinguish a specific one.

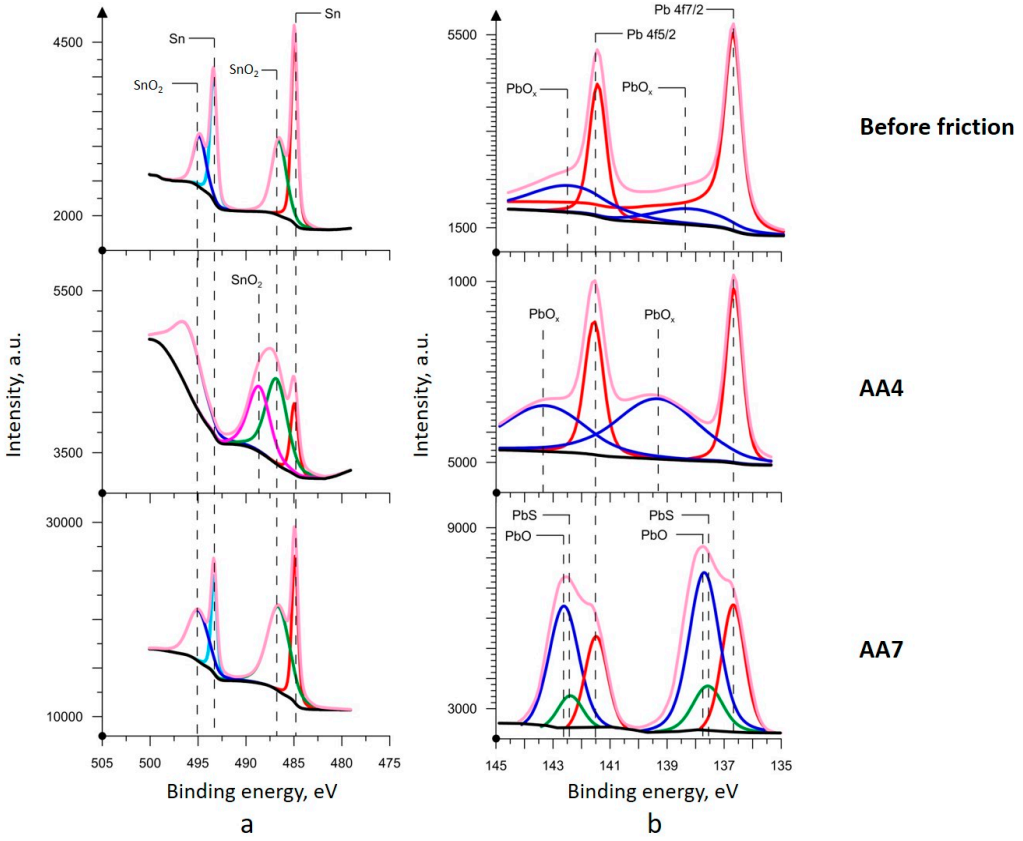

Figure 10. High-resolution XPS spectra of (**a**) Sn and (**b**) Pb.

In contrast to tin, lead in the AA4 alloy was less smeared over the surface, which affected the XPS spectrum (Figure 10b). The metallic lead maintained the binding energy and FWHM and showed higher intensity on the spectrum. The lead oxide line was shifted to greater energies of 139.2 eV, while FWHM increased by 0.5 eV. After friction, the list of lead oxides could be rebalanced, affecting the XPS results in this way.

The XPS spectrum of lead in the $4f_{7/2}$ region of the AA7 alloy differed significantly (Figure 10b). Its deconvolution resulted in three peaks. First, there was a spectral line of metallic lead, the extremum of which retained the binding energy of 136.6 eV and the FWHM parameter. The most intense component was the line, with a peak at 137.7 eV. The line had a much smaller FWHM parameter than in the initial state—1.5 eV, which made it possible to interpret it as a PbO compound [50]. The presence of other oxides was possible due to the higher binding energy. However, lead (II) oxide was determined to be dominant. The third least intense spectrum had a binding energy of 137.5 eV, also indicating the presence of lead Pb^{2+}. The analysis of the 4f5/2 doublet revealed the 4.9 eV (137.5 eV and 142.4 eV) splitting between these peaks. Bond energies and peak shift values are the references for determining the PbS phase [51,52]. Thus, these findings support the EDX results. Like Cu3Sn, PbS is formed at temperatures >600 °C when these components come into contact in the system.

The high-resolution spectra of zinc of all samples shared one pattern (Figure 11a). In the initial state, the ZnO compound dominated on the surface, as evidenced by the peak with a binding energy of 1022.1 eV in the 2p range, which is common for Zn^{2+} ions [53]. The second peak was half as intense and had a binding energy of 1022.7 eV, indicating the presence of metallic zinc [54]. After friction, both samples showed a significant increase in the zinc content on the friction surface. In the alloy AA7, their ratio is approximately 1:1. On the one hand, zinc could be transferred from the lubricant (Table 3). In this case, being free or in a covalent bond, the zinc peak would have been found at lower energies of 1021.6–1022.0 eV. However, zinc peaks were only found at higher binding energies, proving

that zinc was in a metallic bond in the solid solution. Moreover, combined with EDX results, the content of zinc on the surface was beyond the solubility of aluminum, which suggests the non-spontaneous process of zinc precipitation during friction.

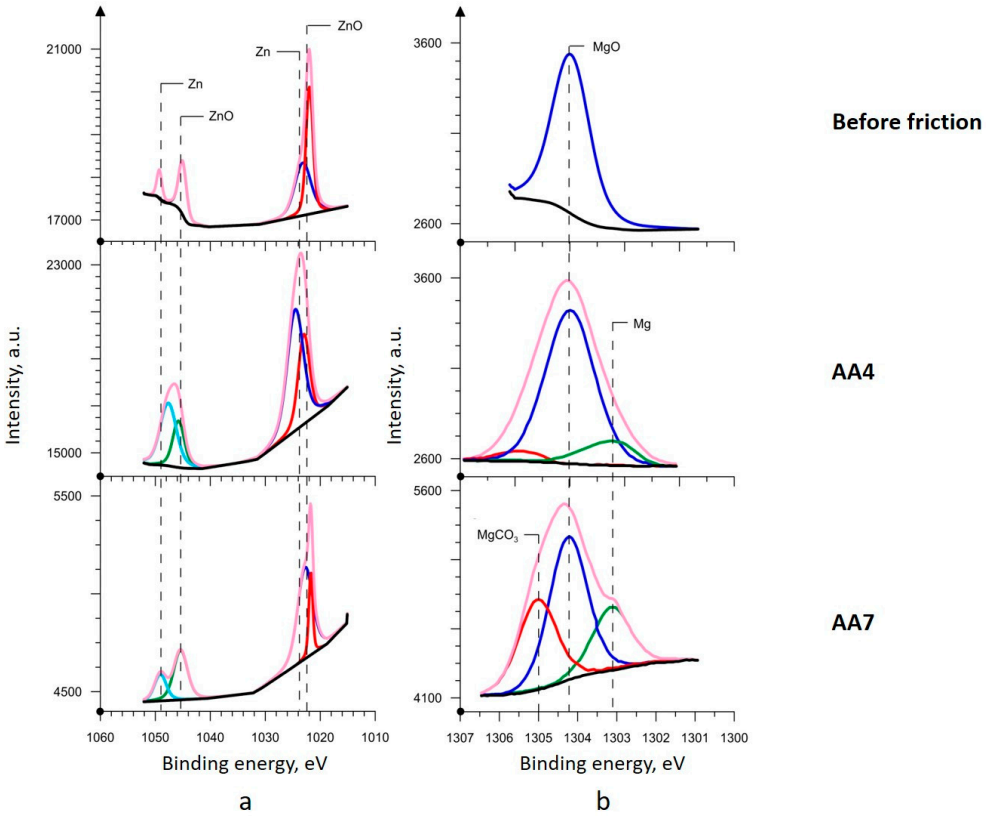

Figure 11. High-resolution XPS spectra of (**a**) Zn and (**b**) Mg.

The magnesium spectrum at the Mg 1s line in the aluminum alloy before friction had one peak with a binding energy of 1304.1 eV, presenting the magnesium ion Mg^{2+}, namely, the MgO oxide (Figure 11b) [55]. Extensive changes were detected on the AA7 friction surface. The approximation of the spectrum resulted in three lines. In addition to the initial MgO peak, a new one at 1303.2 eV was observed, which was identified as Mg^0 [56]. Another peak had a binding energy of 1305.0 eV, which is typical for magnesium carbonate $MgCO_3$ [57]. In the AA4 alloy, the spectrum of magnesium oxide remained dominant, while the peaks related to magnesium and magnesium carbonate had a much lower intensity.

Since the other objects in the tribosystem contained no magnesium, the increase in the intensity of free magnesium cases cannot be explained by mass transfer. Therefore, this is magnesium from the aluminum alloy, which was not fully oxidized. Given that magnesium strongly tends to oxidize, the process could be prevented by a polymerized tribofilm that protects magnesium from contact with air. Furthermore, to form the $MgCO_3$ compound, free magnesium is necessary in the system, which was absent in sufficient quantity. Thus, it could be concluded that magnesium precipitates during friction from the solid solution with the following reaction with oxygen and carbon.

Fitted carbon spectra at the C1s line revealed the main peak at 285.5 eV, indicating the presence of C–C phases (Figure 12a). On the surface before friction, carbon is also detected with a maximum binding energy of 288.3 eV, showing a relatively small amount of its oxide forms. After the tests, the number of carbon bonds in both alloys rose. Firstly, the presence of C–OH hydrocarbon groups with a binding energy of 287.1 $\pm$ 0.3 eV was detected, the intensity of which is noticeably higher in the AA4 alloy. It is directly related

to the oxidation of lubricant residues based on hydrocarbon CH_2 in the microcavities of the surface. The presence of carbonyls (C=O) with a binding energy of 289.7 eV was also observed [58]. The least intense line of the spectrum had a peak at a binding energy of 291.1 eV and can be interpreted either as a π–π satellite, a CF bond [59], a C–H bond [60], or carbon in a CO_3^{2-} bond [61]. The latter case supports the opinion on the presence of $MgCO_3$, while peak intensity correlates with its small content. Thus, it can be concluded that during friction, intense polymerization takes place. Considering the amount of carbon in the tribosystem, it can be assumed that the tribofilms based on polymerized material become the first friction surface after the running-in stage.

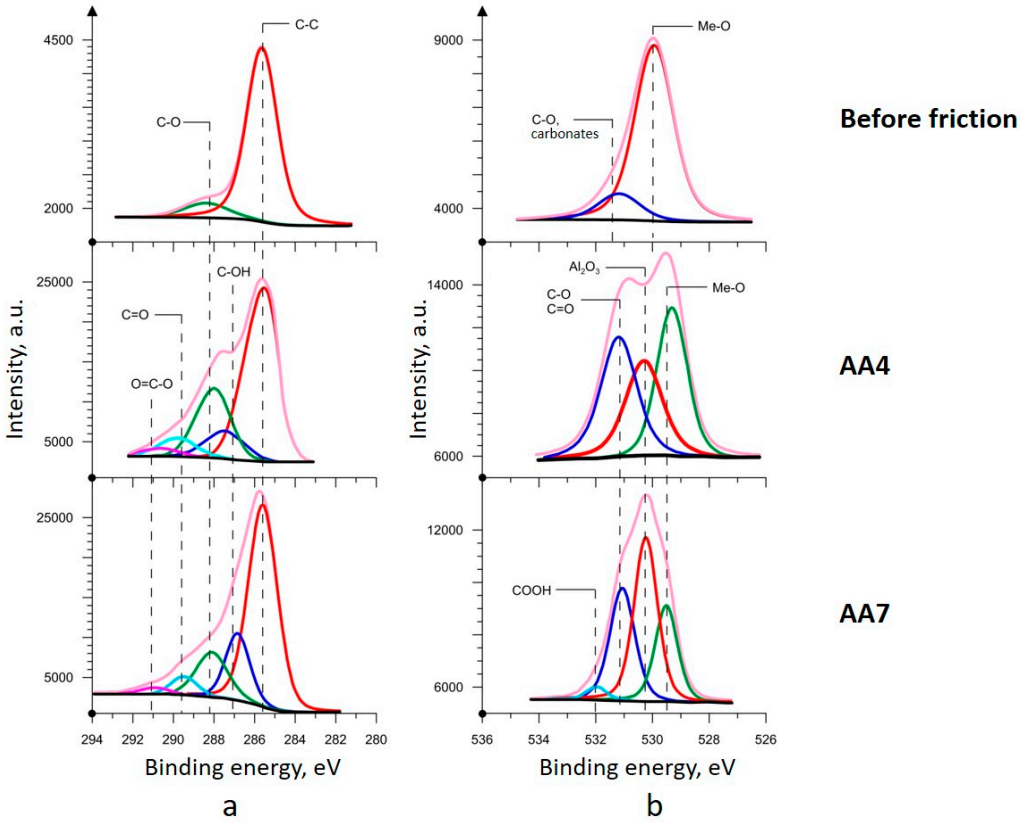

Figure 12. High-resolution XPS spectra of (**a**) C and (**b**) O.

The XPS spectrum of oxygen O1s in the initial state showed the presence of metal oxides at 529.9 eV (Figure 12b). It appears to be linked to the aluminum oxide film. The presence of other oxides of copper, tin, lead, and other metals explains the shift to lower energies. The second line in this spectrum was less intense, had a binding energy of 531.3 eV, and corresponded to various C–O compounds. The O1s spectrum of the AA7 alloy after friction, as in the case of carbon, showed significant oxygen saturation of the surface. After deconvolution, three significant spectra were identified with peak binding energies of 529.5 eV, 530.3 eV, and 531.3 eV. The first one stands for various metal oxides, mainly tin, lead, copper, and other alloying elements. The exception is the most intense peak of an aluminum oxide, which was found at 530.3 eV (Figure 12b). Furthermore, the content of C–O bonds and carbonates increased a lot, as evidenced by the peak at 531.3 eV. Interestingly, the Al_2O_3 peak had the lowest intensity. Smeared soft metals covered large areas of the Al matrix. It may also suggest the formation of polymerized films on the surface, blocking the XPS signal. The XPS spectrum of the AA4 alloy is characterized by a similar set of chemical states of oxygen. This signifies a diminished distribution of soft inclusions and polymerized films throughout the surface, aligning with the EDX results.

Analogous to the other primary constituents of the alloy, prior to experiencing surface friction, silicon predominantly existed in two distinct forms: the elemental state Si^0 and the oxidized form Si^{+4}. The latter is attributable to the generation of an oxide layer composed of silicon dioxide. This is indicated by two lines in the high-resolution Si 2p spectrum with binding energies of 98.9 eV (Si^0) and 103.6 eV (SiO_2) (Figure 13a). In both alloys, after friction, silicon underwent total oxidation, and its metal form was no longer observed. SiO_2 is a harder compound, contributing to the wear resistance of the alloys. At the same time, being brittle, silicon dioxide tends to generate debris acting as abrasive particles.

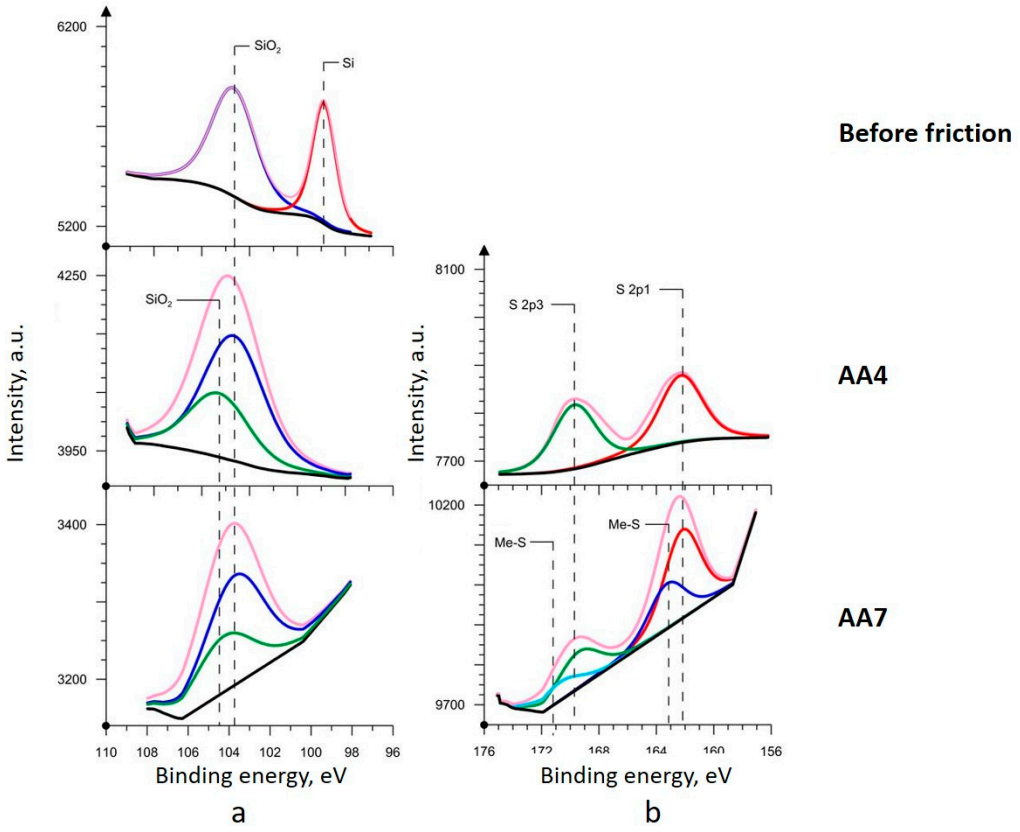

Figure 13. High-resolution XPS spectra of (**a**) Si and (**b**) S.

Sulfur was absent on the surface of the alloys before friction and was found only on friction surfaces, where it was transferred from the lubricant. A study of the high-resolution spectrum of the AA4 alloy made it possible to identify a sulfur peak with a binding energy of 162.1 eV on the characteristic S 2p1 line, as well as a doublet on the S 2p3 line with a binding energy of 169.8 eV, which is typical of elemental sulfur (Figure 13b). The deconvoluted XPS spectra of the AA7 alloy showed one more peak at 163.2 eV on the S 2p1 line and a peak at 171.2 eV on the S 2p3 line. This binding energy was reported for sulfides of various metals [62], including PbS. It confirms the possibility of lead sulfide formation in the tribofilms of the AA7 alloy.

All changes detected by XPS in the alloys after friction compared to the initial state are presented in Table A1. In total, before friction, the alloy elements, carbon and oxygen, formed an average of 16 compounds; after friction, this number increased to 24 (Table A1).

To study the tribofilms in depth, XPS with stepwise ion etching was used. Figure 14 presents the concentration profiles of the elements for both alloys.

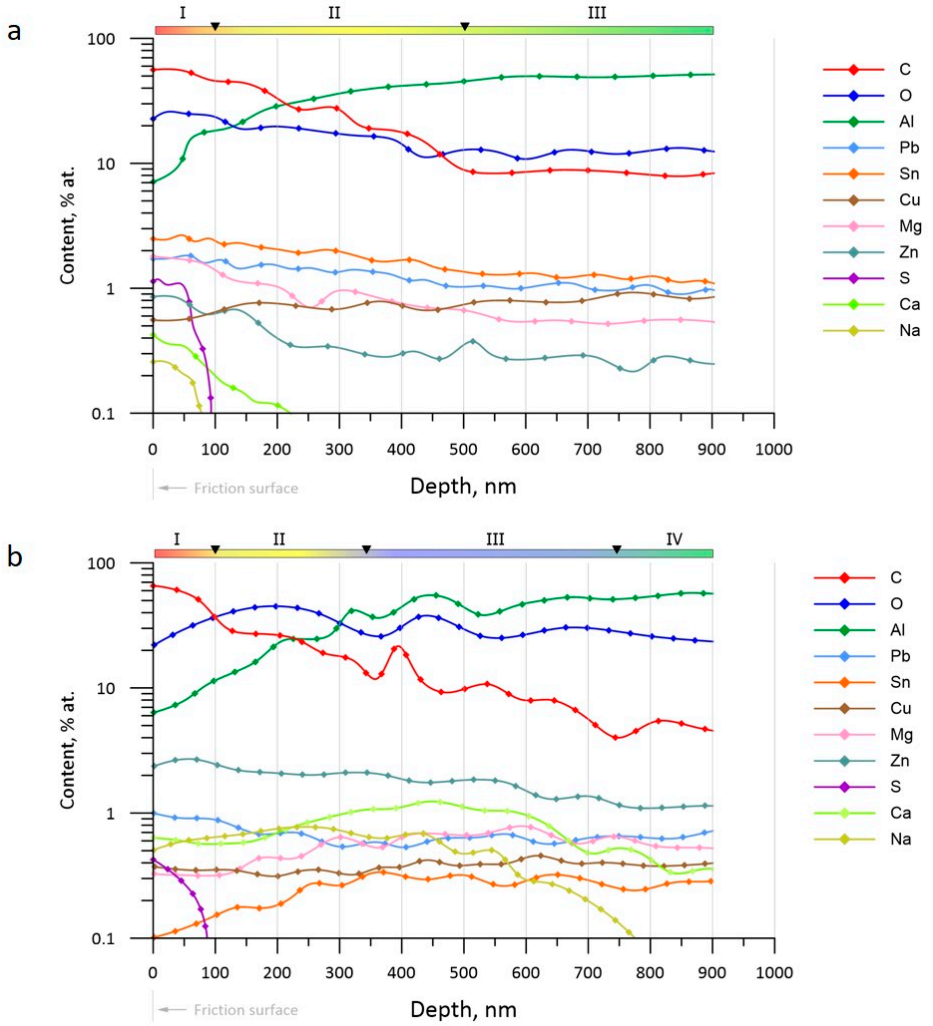

Figure 14. XPS profile of (**a**) the AA7 alloy and (**b**) the AA4 alloy.

The surface layer of the AA7 alloy is largely composed of carbon, oxygen, and their compounds (Figure 14a). At 50 nm depth, their concentrations change approximately equally, and after 100 nm, a more intense drop in carbon concentration is observed. The turning point is observed at a depth of 500 nm when the oxygen concentration begins to exceed the carbon concentration. Both curves are equally decreasing up to 100 nm, which may indicate a quantitative change in a composition consisting of one set of C–O compounds, for example, a polymerized material. This is indirectly confirmed by the change in aluminum concentration that increases sharply after 50 nm. A stable growth in aluminum concentration starts at a depth of 75–80 nm.

Soft metals had the highest concentration on the surface due to intense smearing. There is also a consistent increase in the concentrations of magnesium and zinc. Copper was the only alloying component, the content of which decreased towards the surface.

Elements from the lubricant, such as sulfur, sodium, and others, were only detected on the surface no deeper than 100 nm, except calcium.

In Figure 14a, it was attempted to distinguish three characteristic areas:

1. Polymerized tribofilm, saturated with alloy elements and lubricant additives (I);
2. A transition layer of aluminum oxide enriched with alloy elements (100–500 nm) (II);
3. Plastically deformed matrix (>500 nm) (III).

Oxidized aluminum is typical for each area, as constant deformation and scratching in contact with air take place. The first layer was formed by the polymerization of the

lubricant. Its formation was preceded by the formation of a second layer directly in the alloy, into which some elements were transferred. The formation of the third layer was caused by cold hardening due to shear stresses and deformation, and the oxidation processes were secondary. This layer had increased bearing capacity and hardness to resist deformations.

In the AA4 alloy, carbon remains a predominant element up to 100 nm depth (Figure 14b). From 300 nm to 750 nm, the concentration lines of oxygen and aluminum follow each other, indicating the presence of Al_2O_3. In contrast to lead, tin is almost absent on the surface, and its concentration gradually increases with the depth of research. Zinc and magnesium also had increased concentrations at the surface, but their maximum content is found at some depth from the surface: 75 nm for zinc and 500 nm for magnesium.

Thus, the AA4 tribofilm includes a bit different set of layers (Figure 14b):

1. A polymerized tribofilm (<50 nm) (I);
2. A polymerized and oxidized material (50–300 nm) (II);
3. An aluminum oxide enriched with alloy components and lubricant additives (300–750 nm) (III);
4. A plastically deformed matrix (>750 nm) (IV).

Both alloys are characterized by mass transfer of the alloy elements to the surface (zinc and magnesium), which not only involves them in the formation of the tribofilms but also increases the hardness of the aluminum matrix along with plastic deformation due to dispersion strengthening.

Thus, there are several aspects responsible for the tribological properties of aluminum alloys. These include self-lubrication due to the smearing of soft metals. Hard copper-based inclusions provide oil-retaining relief. Elastoplastic deformation of the surface layer is one of the ways friction energy dissipates. However, the total energy consumption during friction cannot be compensated only by deformation in the surface layers [63]. Therefore, tribochemical processes play an important role in energy dissipation.

Under conditions of mixed friction, zones of high pressure and elevated temperature are formed in the contact zone of surfaces for a short time, which leads to the destruction of the lubricant. As a result, the process of polycondensation occurs when additives, for example, dimer acids, glycols, and other monomers dissolved in the hydrocarbon environment of mineral oils, form long chains of molecules or a polymer film [64,65]. The process involves a change in the state of aggregation of a substance from a liquid to a solid film and, therefore, is accompanied by a decrease in entropy. As the tribopolymer film forms, the intensity of friction in a local area decreases due to limiting the contact of metal surfaces. At the same time, the tribosystem is capable of supporting the process of tribopolymerization. As the polymer wears out, the intensity of friction increases, and so does temperature, which leads to the formation of a new polymer film. Its formation on the surface is due to chemisorption due to the attachment of active radicals of the high-molecular compounds to the metal.

The subsurface layer to a depth of at least 1 μm undergoes elastoplastic deformation during friction, which is characterized by the movement and accumulation of vacancies and dislocations in this area [66]. The dislocation density is one to two orders of magnitude greater than in the equilibrium state. Moreover, surface deformation can reach a significant value without destruction, provided that a fragmentary dislocation structure is formed. The formation of fragments is a spontaneous process in which the density of dislocations along the boundaries is several orders of magnitude higher than the density of dislocations inside the fragments. With further deformation, dislocations move along the boundaries. Ceteris paribus, such inhomogeneity leads to a decrease in entropy and an increase in the free energy of the deformed area compared to the fragmentless state, which corresponds to self-organization [67,68]. Earlier, it was shown that dislocation glide plays an important role during the friction of Hadfield steel [69], another material capable of a non-spontaneous process of austenite to martensite transition under mechanical impact with high dislocation density that generates a short-range stress field promoting strain hardening.

The constant physical impact caused an interatomic bond rupture in the crystal lattice, which led to mechanical activation and increased reactivity. Exposed surfaces are passivated quickly by an oxide film formation. The chains of accumulated microstructural defects became another channel for the diffusion of the elements transferred to the alloy.

The formation of carboxylic compounds in metals, in particular aluminum, can be considered the result of mechanical activation. Such compounds have great hardness and wear resistance.

High mechanical stresses, increased density of vacancies and dislocations, destruction of interatomic bonds, and the resulting temperature gradient caused the loss of thermodynamic equilibrium of the surface layer of the alloys. This volume of material is the main area of dissipation of the friction energy. Part of this energy is consumed by linear processes such as thermal conductivity, triboluminescence, electron emission, plasma formation, electrical conductivity, and others. Excess energy may result in seizures of the rubbing body or self-organization through tribolfilm formation. A non-equilibrium state is a necessary condition for self-organization during friction that shifts the constants of chemical reactions and increases chemical activity. For instance, XPS analysis revealed some metal oxides that had unusual binding energies. This could be caused by the presence on the surface of stable oxides of non-stoichiometric composition, which were also formed as a result of friction.

One of the main features of the formed tribofilms was the precipitation of magnesium on the friction surface, which was initially present only in the solid solution with aluminum and soft inclusions. Having low electronegativity, magnesium was instantly oxidized. Further mechanical activation in a carbon-rich environment during friction led to $MgCO_3$ formation.

The aluminum alloys were produced by casting with the following annealing. Therefore, the alloys were in an equilibrium state. After friction, areas with increased Mg and Zn concentrations above the solubility threshold were observed, confirming that a non-spontaneous process of precipitation took place. Comparing the wear of the two alloys, it can be concluded that the Mg-related process is more beneficial for wear reduction than the Zn-related process. This is due to the initial difference in magnesium alloying: the AA7 alloy contained 1.5% Mg, while the AA4 alloy contained only 0.5% Mg. Thus, the wear intensity of the alloys may be linked to the ability of magnesium to precipitate from a solid solution.

The AA4 tribolfilm contains an increased content of zinc. The solubility of zinc in aluminum is less than 4%. It also indicates that there was a supersaturated solid solution with zinc on the surface. That fact proves the non-equilibrium state of the alloys necessary for self-organization. Given the worst wear rate of the AA4 sample, it is hard to claim that zinc precipitation is insufficient to reduce the wear rate. Less pronounced, this phenomenon was observed in the AA7 alloy as well. Therefore, this process is typical for the alloys and is initiated during self-organization during friction. However, for wear reduction, magnesium precipitation is favorable. Thus, it can be concluded that self-organization in alloys can occur in different ways and depends on the initial composition of the components and their quantitative ratio.

The precipitation of the elements is preceded by a destabilization of the equilibrium of the surface layer due to an increase in the concentration of these elements due to the diffusion of atoms. A part of the mechanical energy generated during friction turns into thermal energy, causing heating of the contacting area. Due to high heating and cooling rates, temperature gradients are formed that intensify the existing stress fields. Significant diffusion flows of atoms arise in depth when atoms move from one equilibrium position at the nodes of the crystal lattice to another. The thickness of the region of diffusion movement can reach tens of microns [70]. The resulting diffusion vector is directed towards the maximum values of temperature and pressure, i.e., towards the contact of rubbing surfaces. Vacancies in the surface layer have a positive effect on the intensity of diffusion transitions. This also leads to the combination of several individual point defects into one,

which is thermodynamically beneficial since it is accompanied by a decrease in the Gibbs free energy in the system.

4. Conclusions

Under conditions of mixed friction with steel according to the kinematic shaft-block scheme, seven experimental aluminum alloys with different tin contents were studied. The tribofilms of the alloys that showed the best and worst tribological properties were studied by EDX and XPS to analyze the changes that occurred during friction and evaluate their influence on wear rate.

Following friction, a total of eight novel bonds with alloy components were identified on the surface. Specifically, the formation of regions containing a supersaturated solid solution of aluminum combined with magnesium (AA7 alloy) and aluminum with zinc (AA4 alloy) was verified, along with the subsequent precipitation of these elements from the solid solution. These processes are not spontaneous and contribute to a reduction in the wear rate.

After friction, tricopper stannide and lead sulfide in the tribofilms were found. Normally, these reactions require a temperature >600 °C. Such a temperature on the friction surface was not achieved. Therefore, the formation of these compounds is also a result of non-spontaneous processes.

The friction surface and the subsurface layer acted as a gradient structure. A polymerized lubricant layer covered the solid alumina and formed the basis of the tribofilm. This layer was in direct contact with the steel counterbody, reducing the seizure probability. Lower, there was a zone where tribochemical processes and the diffusion of elements to the surface occurred. Next, a plastically deformed layer with increased hardness was observed.

Thus, the adaptation of material during friction goes not only through mechanical running-in but also through self-organization processes and tribofilm formation. Owing to this ability, the AA7 aluminum alloy showed two times higher wear resistance and 7.5 times less counterbody wear than the antifriction bronze.

Author Contributions: Conceptualization, I.G. and A.M.; methodology, P.P. and A.A.O.; software, E.K.; validation, I.G., E.K. and A.M.; formal analysis, P.P.; investigation, P.P. and E.K.; resources, I.G. and S.N.G.; data curation, I.G.; writing—original draft preparation, P.P.; writing—review and editing, I.G. and P.P.; visualization, P.P.; supervision, I.G.; project administration, S.N.G.; funding acquisition, S.N.G. All authors have read and agreed to the published version of the manuscript.

Funding: This work was supported financially by the Ministry of Science and Higher Education of the Russian Federation (project No. FSFS-2021-0003).

Data Availability Statement: The data presented in this study are available on request from the corresponding author.

Acknowledgments: This study was carried out on the equipment of the Center of Collective Use "State Engineering Center" of the MSUT "STANKIN" (project 075-15-2021-695, unique id RF----2296.61321X0013).

Conflicts of Interest: The authors declare no conflict of interest.

Appendix A

The list of bonds found by XPS analysis in tribofilms of both the AA7 and AA4 alloys is presented in Table A1.

Table A1. The results of the XPS study of the AA7 and the AA4 alloys.

Alloy	Line	State					
		Before Friction			After Friction		
		Binding Energy, eV	Compound	Content, % Mass.	Binding Energy, eV	Compound	Content, % Mass.
AA7	Al 2p	72.9	Al^0	12.57	72.9	Al^0	4.21
		75.7	Al_2O_3	49.24	75.7	Al_2O_3	3.54
			-		74.6	Al–OC	1.87
	C 1s	285.7	C–C	7.88	285.7	C–C	26.41
		288.3	C–O	2.64	287.1	C–OH	3.22
			-		288.3	C–O	8.74
			-		289.5	C=O	4.79
			-		291.1	O=C–O	3.53
	Sn 3d	484.8	Sn^0	1.33	484.8	Sn^0	5.34
		487.1	SnO	1.22	487.1	SnO	3.10
	Pb 4f	136.6	Pb^0	0.89	136.6	Pb^0	4.61
		137.7	PbO_x	1.10	137.7	PbO	6.45
			-		137.5	PbS	1.62
	Zn 2p	1022.7	Zn^0	0.42	1022.7	Zn^0	0.79
		1022.1	ZnO	0.10	1022.1	ZnO	0.29
	Mg 1s	1304.1	MgO	0.40	1304.1	MgO	2.15
			-		1303.1	Mg^0	1.00
			-		1305.0	$MgCO_3$	1.12
	Cu 2p	932.9	Cu_2O	1.17	933.7	CuO	0.73
			-		936.1	CuO	0.32
	Si 2p	99.8	Si^0	0.84	103.6	SiO_2	0.59
		103.8	SiO_2	2.52	-		
	O 1s	530.1	Me–O	12.33	529.5	Me–O	6.04
		531.5	C–O	2.95	530.3	Al_2O_3	2.09
			-		531.3	C–O, C=O	5.09
AA4	Al 2p	72.9	Al^0	11.31	72.9	Al^0	6.26
		75.7	Al_2O_3	45.75	75.7	Al_2O_3	3.42
					74.6	Al–OC	1.94
	C 1s	285.7	C–C	7.88	285.7	C–C	26.21
		288.3	C–O	2.64	287.1	C–OH	4.67
			-		288.3	C–O	7.91
			-		289.5	C=O	3.77
			-		291.1	O=C–O	2.42
	Sn 3d	484.8	Sn^0	2.15	484.8	Sn^0	0.29
		487.1	SnO_2	1.86	487.1	SnO_2	0.43
			-		488.0	SnO_2	0.38
	Pb 4f	136.6	Pb^0	1.05	136.6	Pb^0	6.07
		137.7	PbO_x	1.66	139.4	PbO_x	2.95
	Zn 2p	1022.7	Zn^0	0.81	1022.7	Zn^0	1.41
		1022.1	ZnO	0.24	1022.1	ZnO	1.36
	Mg 1s	1304.1	MgO	0.33	1304.1	MgO	0.43
			-		1303.1	Mg^0	0.11
	Cu 2p	932.9	Cu_2O	1.34	932.6	Cu/Cu_2O	1.17
			-		933.1	CuO	2.11
	Si 2p	99.8	Si^0	0.94	103.6	SiO	1.37
		103.8	SiO_2	2.11	-		
	O 1s	103.8	SiO_2	2.46	529.5	Me–O	5.73
		530.1	Me–O	13.34	530.3	Al_2O_3	10.40
		531.5	C–O	2.16	531.3	C–O, C=O	7.04

References

1. Holmberg, K.; Andersson, P.; Erdemir, A. Global energy consumption due to friction in passenger cars. *Tribol. Int.* **2012**, *47*, 221–234. [CrossRef]
2. Kumar, S.; Kumar, V.; Singh, A.K. Influence of lubricants on the performance of journal bearings—A review. *Tribol.-Mater. Surf. Interfaces* **2020**, *14*, 67–78. [CrossRef]
3. Gao, Q.; Chen, W.; Lu, L.; Huo, D.; Cheng, K. Aerostatic bearings design and analysis with the application to precision engineering: State-of-the-art and future perspectives. *Tribol. Int.* **2019**, *135*, 1–17. [CrossRef]
4. Zemtsova, E.G.; Arbenin, A.Y.; Sidorov, Y.V.; Morozov, N.F.; Korusenko, P.M.; Semenov, B.N.; Smirnov, V.M. The use of carbon-containing compounds to prepare functional and structural composite materials: A review. *Appl. Sci.* **2022**, *12*, 9945. [CrossRef]
5. Mironov, A.; Gershman, I.; Gershman, E.; Podrabinnik, P.; Kuznetsova, E.; Peretyagin, P.; Peretyagin, N. Properties of Journal Bearing Materials That Determine Their Wear Resistance on the Example of Aluminum-Based Alloys. *Materials* **2021**, *14*, 535. [CrossRef] [PubMed]
6. Sevostyanov, N.V.; Bolshakova, A.N.; Bolsunovskaya, T.A.; Burkovskaya, N.P. Tribotechnical Properties of Nickel Based Cermet Materials. *J. Frict. Wear.* **2021**, *42*, 335–339. [CrossRef]
7. Dong, W.; Yang, X.; Song, F.; Wu, M.; Zhu, Y.; Wang, Z. Anti-friction and wear resistance analysis of cemented carbide coatings. *Int. J. Adv. Manuf. Technol.* **2022**, *122*, 2795–2821.
8. Polmear, I.J.; St. John, D.H.; Nie, J.-F.; Qian, M. *Light Alloys Metallurgy of the Light Metals*, 5th ed.; Elsevier/Butterworth-Heinemann: Oxford, UK, 2017; 537p.
9. Prasad, S.V.; Asthana, R. Aluminium Metal-Matrix Composites for Automotive Applications: Tribological Considerations. *Tribol. Lett.* **2004**, *17*, 445–453. [CrossRef]
10. Huang, S.; Zhu, B.; Zhang, Y.; Liu, H.; Wu, S.; Xie, H. Microstructure Comparison for AlSn20Cu Antifriction Alloys Prepared by Semi-Continuous Casting, Semi-Solid Die Casting, and Spray Forming. *Metals* **2022**, *12*, 1552. [CrossRef]
11. Kalogeropoulos, A.; Kalogeropoulou, A.; Theodorakakos, A.; Lelidakis, G. Experimental investigation of an Al-Cu alloy as an alternative cylinder liner material for internal combustion engines. *Mater. Today Proc.* **2020**, *27*, 2098–2104.
12. Cui, S.; Sun, P.; Li, X.; Huang, H.; Gao, K. Oxidation and tribological behaviors of Cu-Al, Cu-Sn, and Cu-Zn solid solutions. *Results Phys.* **2019**, *12*, 2306–2315.
13. Yang, M.; Ding, J.; Hu, Z.; Peng, Y.; Wang, R.; Jiang, W. Investigation on microstructure and tribological properties of ex situ nano-SiCp reinforced Al-Cu matrix composite prepared by the stirring-casting process. *J. Alloys Compd.* **2020**, *848*, 156454.
14. Sohag, M.A.Z.; Gupta, P.; Kondal, N.; Kumar, D.; Singh, N.; Jamwal, A. Effect of ceramic reinforcement on the microstructural, mechanical and tribological behavior of Al-Cu alloy metal matrix composite. *Mater. Today Proc.* **2020**, *21*, 1407–1411. [CrossRef]
15. Jain, S.; Naveen, L.; Kumar, V.; Samal, S. Effect of Ni and Si alloying elements on the phase evolution, mechanical properties, tribological behaviour of Al–Cu alloys. *Mater. Chem. Phys.* **2023**, *297*, 127421. [CrossRef]
16. Carlton, H.; Huitink, D.; Liang, H. Tribochemistry as an Alternative Synthesis Pathway. *Lubricants* **2020**, *8*, 87. [CrossRef]
17. Morina, A.; Neville, A. Tribofilms: Aspects of formation, stability and removal. *J. Phys. D Appl. Phys.* **2007**, *40*, 5476. [CrossRef]
18. Gellman, A.J.; Spencer, N.D. Surface chemistry in tribology. *Proc. Inst. Mech. Eng. Part J J. Eng. Tribol.* **2002**, *216*, 443–461. [CrossRef]
19. Bowden, F.P.; Tabor, D. The area of contact between stationary and moving surfaces. *Proc. R. Soc. Lond.* **1939**, *169*, 391–413. [CrossRef]
20. Bershadskiy, N.Y. *Structural Thermodynamics of Tribosystem*; Znanie: Kiev, Russia, 1990. (In Russian)
21. Gershman, J.S.; Bushe, N.A. Thin films and self-organization during friction under the current collection conditions. *Surf. Coat* **2004**, *186*, 405–411. [CrossRef]
22. Gershman, I.S.; Mironov, A.E.; Gershman, E.I.; Fox-Rabinovich, G.S.; Veldhuis, S.C. Self-organization during friction of slide bearing antifriction materials. *Entropy* **2015**, *17*, 7967–7978. [CrossRef]
23. Fox-Rabinovich, G.; Gershman, I.S.; Locks, E.; Paiva, J.M.; Endrino, J.L.; Dosbaeva, G.; Veldhuis, S. The Relationship between Cyclic Multi-Scale Self-Organized Processes and Wear-Induced Surface Phenomena under Severe Tribological Conditions Associated with Buildup Edge Formation. *Coatings* **2021**, *11*, 1002. [CrossRef]
24. Naderi, M. On the Evidence of Thermodynamic Self-Organization during Fatigue: A Review. *Entropy* **2020**, *22*, 372. [CrossRef] [PubMed]
25. Nakayama, K.; Martin, J.M. Tribochemical reactions at and in the vicinity of a sliding contact. *Wear* **2006**, *26*, 235–240. [CrossRef]
26. Yin, C.H.; Liang, Y.L.; Liang, Y.; Li, W.; Yang, M. Formation of a self-lubricating layer by oxidation and solid-state amorphization of nano-lamellar micro-structures during dry sliding wear tests. *Acta Mater.* **2019**, *166*, 208–220. [CrossRef]
27. Andrade, E.; Randall, R. The Rehbinder effect. *Nature* **1949**, *164*, 1127. [CrossRef]
28. Yusuke, O.; Jingxiang, X.; Naoki, T.; Kenta, A.; Satoshi, S.; Yang, W.; Nobuki, O.; Takahiro, H.; Koshi, A.; Momoji, K. Self-Formed Double Tribolayers Play Collaborative Roles in Achieving Superlow Friction in an Aqueous Environment. *J. Phys. Chem. C* **2020**, *124*, 8295–8303. [CrossRef]
29. Kuzharov, A.A.; Luk'yanov, B.S.; Kuzharov, A.S. Tribochemical transformations of glycerol. *J. Frict. Wear* **2016**, *37*, 337–345. [CrossRef]
30. Wang, B.; Qiu, F.; Barber, G.C.; Zou, Q.; Wang, J.; Guo, S.; Yongfeng, Y.; Jiang, Q. Role of nano-sized materials as lubricant additives in friction and wear reduction: A review. *Wear* **2022**, *490*, 204206. [CrossRef]

31. Luiz, J.F.; Spikes, H. Tribofilm formation, friction and wear-reducing properties of some phosphorus-containing antiwear additives. *Tribol. Lett.* **2020**, *68*, 75. [CrossRef]
32. Waqas, M.; Zahid, R.; Bhutta, M.U.; Khan, Z.A.; Saeed, A. A review of friction performance of lubricants with nano additives. *Materials* **2021**, *14*, 6310. [CrossRef]
33. Dawczyk, J.; Morgan, N.; Russo, J.; Spikes, H. Film thickness and friction of ZDDP tribofilms. *Tribol. Lett.* **2019**, *67*, 34. [CrossRef]
34. Gershman, I.; Bushe, N. Elements of thermodynamics and self-organization during friction. In *Self-Organization during Friction: Advanced Surface Engineered Materials and Systems Designed*, 1st ed.; Fox-Rabinovich, G., Totten, G.E., Eds.; CRC Press, Taylor and Francis Group: Boca Raton, FL, USA, 2006; pp. 13–58.
35. Klamecki, B.E. A thermodynamic model of friction. *Wear* **1980**, *63*, 113–120. [CrossRef]
36. Klimontovich, Y.L. *Introduction to the Physics of Open Systems*; Yanus: Moscow, Russia, 2002; 284p.
37. Genovese, A.; D'Angelo, G.A.; Sakhnevych, A.; Farroni, F. Review on Friction and Wear Test Rigs: An Overview on the State of the Art in Tyre Tread Friction Evaluation. *Lubricants* **2020**, *8*, 91. [CrossRef]
38. Maruyama, B.; Ohuchi, F.S. H_2O catalysis of aluminum carbide formation in the aluminum-silicon carbide system. *J. Mater. Res.* **1991**, *6*, 1131–1134. [CrossRef]
39. Popoola, O.O.; Kriven, W.M. Interfacial structure and chemistry in a ceramic/polymer composite material. *J. Mater. Res.* **1992**, *7*, 1545–1552. [CrossRef]
40. Dubé, C.E.; Workie, B.; Kounaves, S.P.; Robbat, A.; Aksub, M.L.; Davies, G. Electrodeposition of metal alloy and mixed oxide films Using a single-precursor tetranuclear copper-nickel complex. *J. Electrochem. Soc.* **1995**, *142*, 3357. [CrossRef]
41. Wang, D.; Miller, A.C.; Notis, M.R. XPS study of the oxidation behavior of the Cu3Sn intermetallic compound at low temperatures. *Surf. Interface Anal.* **1996**, *24*, 127–132. [CrossRef]
42. Kaldas, M.L.; Cooper, P.A.; Sodhi, R. Oxidation of wood components during chromated copper arsenate (CCA-C) fixation. *J. Wood Chem. Technol.* **1998**, *18*, 53–67. [CrossRef]
43. Célerier, S.; Morisset, S.; Batonneau-Gener, I.; Belin, T.; Younes, K.; Batiot-Dupeyrat, C. Glycerol dehydration to hydroxyacetone in gas phase over copper supported on magnesium oxide (hydroxide) fluoride catalysts. *Appl. Catal. A Gen.* **2018**, *557*, 135–144. [CrossRef]
44. Gaarenstroom, S.W.; Winograd, N.J.T.J. Initial and final state effects in the ESCA spectra of cadmium and silver oxides. *J. Chem. Phys.* **1977**, *67*, 3500–3506. [CrossRef]
45. Zhang, H.; Li, X.; Yao, P.; Wen, L.; Zhu, Y.; He, X.; Yang, G. Microstructure evolution and mechanical properties of Cu-Sn intermetallic joints subjected to high-temperature aging. *Mater. Charact.* **2022**, *186*, 111791. [CrossRef]
46. Junior, P.R.C.A.; Pukasiewicz, A.G.M. Evaluation of microstructure, mechanical and tribological properties of a Babbitt alloy deposited by arc and flame spray processes. *Tribol. Int.* **2019**, *131*, 148–157. [CrossRef]
47. Thomas III, J.H.; Sharma, S.P. An XPS/AES study of films on electroplated Co–Sn alloy. *JVSTA J. Vac. Sci. Technol.* **1978**, *15*, 1706–1711. [CrossRef]
48. Badrinarayanan, S.; Mandale, A.B.; Gunjikar, V.G.; Sinha, A.P.B. Mechanism of high-temperature oxidation of tin selenide. *J. Mater. Sci.* **1986**, *21*, 3333–3338. [CrossRef]
49. Bertrand, P.A.; Fleischauer, P.D. X-ray photoelectron spectroscopy study of the surface adsorption of lead naphthenate. *JVSTA J. Vac. Sci. Technol.* **1980**, *17*, 1309–1314. [CrossRef]
50. Taylor, J.A.; Perry, D.L. An X-ray photoelectron and electron energy loss study of the oxidation of lead. *JVSTA J. Vac. Sci. Technol.* **1984**, *2*, 771–774. [CrossRef]
51. Pederson, L.R. Two-dimensional chemical-state plot for lead using XPS. *J. Electron Spectrosc. Relat. Phenom.* **1982**, *28*, 203–209. [CrossRef]
52. Kovalev, A.I.; Wainstein, D.L.; Rashkovskiy, A.Y.; Osherov, A.; Golan, Y. Size shift of XPS lines observed from PbS nanocrystals. *Surf. Interface Anal.* **2010**, *42*, 850–854. [CrossRef]
53. Ali, H.A.; Iliadis, A.A.; Mulligan, R.F.; Cresce, A.V.W.; Kofinas, P.; Lee, U. Properties of self-assembled ZnO nanostructures. *Solid State Electron.* **2002**, *46*, 1639–1642. [CrossRef]
54. Zanoni, R.; Aurora, A.; Cattaruzza, F.; Decker, F.; Fastiggi, P.; Menichetti, V.; Tagliatesta, P.; Capodilupo, A.L.; Lembo, A. Metalloporphyrins as molecular precursors of electroactive hybrids: A characterization of their actual electronic states on Si (100) and (111) by AFM and XPS. *Mater. Sci. Eng. C* **2007**, *27*, 1351–1354. [CrossRef]
55. Cui, W.; Li, P.; Wang, Z.; Zheng, S.; Zhang, Y. Adsorption study of selenium ions from aqueous solutions using MgO nanosheets synthesized by ultrasonic method. *J. Hazard. Mater.* **2018**, *341*, 268–276. [CrossRef]
56. Hosking, N.C.; Ström, M.A.; Shipway, P.H.; Rudd, C.D. Corrosion resistance of zinc–magnesium coated steel. *Corros. Sci.* **2007**, *49*, 3669–3695. [CrossRef]
57. De Wit, F.M.; Mol, J.M.C.; Terryn, H.; De Wit, J.H.W. The influence of chemical pre-treatment and magnesium surface enrichment on bonding of succinic acid molecules to aluminium alloy. *J. Adhes. Sci. Technol.* **2008**, *22*, 1089–1104. [CrossRef]
58. Bournel, F.; Laffon, C.; Parent, P.; Tourillon, G. Adsorption of some substituted ethylene molecules on Pt (111) at 95 K Part 1: NEXAFS, XPS and UPS studies. *Surf. Sci.* **1996**, *350*, 60–78. [CrossRef]
59. Cardinaud, C.; Rhounna, A.; Turban, G.; Grolleau, B. Contamination of Silicon Surfaces Exposed to CHF 3 Plasmas: An XPS Study of the Film and the Film-Surface Interface. *J. Electrochem. Soc.* **1988**, *135*, 1472. [CrossRef]

60. Cherkashinin, G.; Nikolowski, K.; Ehrenberg, H.; Jacke, S.; Dimesso, L.; Jaegermann, W. The stability of the SEI layer, surface composition and the oxidation state of transition metals at the electrolyte–cathode interface impacted by the electrochemical cycling: X-ray photoelectron spectroscopy investigation. *Phys. Chem.* **2012**, *14*, 12321–12331. [CrossRef] [PubMed]
61. Stipp, S.L.S. Where the bulk terminates: Experimental evidence for restructuring, chemibonded OH^- and H^+, adsorbed water and hydrocarbons on calcite surfaces. *Mol. Simul.* **2002**, *28*, 497–516. [CrossRef]
62. Laajalehto, K.; Kartio, I.; Nowak, P. XPS study of clean metal sulfide surfaces. *Appl. Surf. Sci.* **1994**, *81*, 11–15. [CrossRef]
63. Gane, N.; Skinner, J. The generation of dislocations in metals under a sliding contact and the dissipation of frictional energy. *Wear* **1973**, *25*, 381–384. [CrossRef]
64. Furey, M.J.; Kajdas, C.; Ward, T.C.; Hellgeth, J.W. Thermal and catalytic effects on tribopolymerization as a new boundary lubrication mechanism. *Wear* **1990**, *136*, 85–97. [CrossRef]
65. Furey, M.J. The formation of polymeric films directly on rubbing surfaces to reduce wear. *Wear* **1973**, *26*, 369–392. [CrossRef]
66. Hu, Y.; Liu, H.; Fujii, H.; Ushioda, K.; Araki, H.; Sugita, K.; Liu, K. Vacancy-induced θ′ precipitation during ultrasonic-affected friction stir welding of Al–Cu alloy. *J. Mater. Sci.* **2020**, *55*, 14626–14641. [CrossRef]
67. Garbar, I.I. Some patterns of metal structure formation during friction. *J. Frict. Wear.* **1981**, *2*, 1076–1084. (In Russian)
68. Rybin, A.A. *Large Plastic Deformations and Destruction of Metals*; Metallurgia: Moscow, Russia, 1986; 224p. (In Russian)
69. Lychagin, D.V.; Filippov, A.V.; Kolubaev, E.A.; Novitskaia, O.S.; Chumlyakov, Y.I.; Kolubaev, A.V. Dry sliding of Hadfield steel single crystal oriented to deformation by slip and twinning: Deformation, wear, and acoustic emission characterization. *Tribol. Int.* **2018**, *119*, 1–18. [CrossRef]
70. Wang, X.; Mao, D.; Wei, X.; Li, J.; Meng, H.; Wang, W. Sliding friction induced atom diffusion in the deformation layer of 0.45% C steel rubbed against Tin alloy. *Tribol. Int.* **2013**, *64*, 128–134. [CrossRef]